TÜBİTAK

Turkish Journal of Earth Sciences

http://journals.tubitak.gov.tr/earth/

Research Article

Turkish J Earth Sci
(2021) 30: 247-267

doi:10.3906/yer-2008-2

Stacked debris flows offshore Sakarya Canyon, western Black Sea: morphology, seismic characterization and formation processes

Derman DONDURUR[1], **Aslıhan NASIF**[1,2,*]

[1]Institute of Marine Sciences and Technology, Dokuz Eylül University, İzmir, Turkey

[2]The Graduate School of Natural and Applied Sciences, Dokuz Eylül University, İzmir, Turkey

Received: 03.08.2020 • **Accepted/Published Online:** 02.12.2020 • **Final Version:** 22.03.2021

Abstract: Analysis of ca. 1400 km of multichannel seismic data indicate that the distal part of the Sakarya Canyon within the continental rise is an unstable region with sediment erosion. Fourteen buried debris flows (DB1–DB14), in the stacked form within Plio–Quaternary sediments between 1400 and 1950 m water depth, were observed in the surveyed area. Their run-out distances range from 3.8 to 24.4 km. The largest debris flow DB10 affects ca. 225 km^2 surficial area transporting ca. 15 km^3 of sediment in S to N direction.

The debris flows in the area are considered as gravity flows of unconsolidated sediments mobilized due to the excess pore pressures occurred in the unconsolidated shallow sediments arising from the high sedimentation rate. We also suggest that extensive seismic activity of North Anatolian Fault (NAF) located ca. 140 km south of the of the study area along with the possible local fault activity is also a significant triggering factor for the flows. The stacked form of the debrites indicates that the excess pore pressure conditions are formed periodically over the time in the continental rise, which makes the region a potentially unstable area for the installation of offshore engineering structures.

Key words: Western Black Sea, Sakarya Canyon, debris flow, seismic reflection, excess pore pressures

1. Introduction

Continental slopes are the areas extending from shallow shelf areas to deep abyssal plains with a relatively high bathymetric gradient. The high inclination of the seabed along the continental slopes causes specific sedimentological processes such as slump and slides or gravitational flows (turbidity and debris flows) due to the effect of earthquakes, bottom currents or gravitational load (e.g., Mulder et al., 2009; Loncke et al., 2009; Mouchot et al., 2010; Savini and Corselli, 2010; Dondurur et al., 2013). These sedimentary processes on the continental slopes are the main mechanism that distributes the shelf and upper continental slope sediments to downslope towards the abyssal depths. As a result of sedimentation and erosional processes along the continental margins, different types of sediment deposits such as terrigenous sediments, turbidites, contourites, pelagic/hemipelagic sediments and mass transport deposits (MTD) occur (e.g., Hernández–Molina et al., 2008; Domzig et al., 2009; Loncke et al., 2009). High resolution seismic and bathymetric measurements allow us to study different types of sediment accumulations deposited at various depths from the seabed, observed both in shallow and deep parts of the continental margins. Submarine slump and slides occur as a result of sudden and rapid displacement of unconsolidated sediments in areas where the seafloor inclination is relatively high such as along the steep slopes or canyon walls typically due to the triggering by the seismic activity (Hampton et al., 1996). The term "gravity flow" or synonymously used "density flow", which was first proposed by Middleton and Hampton (1973), is defined as the flow of sediment or sediment-liquid mixture under the effect of gravity. The material transported is denser than the surrounding liquid, and it moves down the slope due to its own gravity (Drago, 2002). Sediment transport capacity is quite high during the sliding or flowing, and sometimes 20.000 km^3 of sliding material can be transported over considerably long distances (typically hundreds of km) (Hampton et al., 1996; Çukur et al., 2016).

Downslope mass movements occur mainly in the form of (i) slides, (ii) slumps, and (iii) debris flows (Moscardelli and Wood, 2008). Slides are defined as rigid sediment volumes that glide on a planar surface and do not show any internal deformation, and they usually occur in low gradient slope (usually less than 4°) regions. Slumps, on the other hand, move along a concave sliding plane, similar

* Correspondence: aslihan.nasif@deu.edu.tr

to those observed on land, and due to this rotational movement, internal deformation occurs within the sliding material (Shanmugam, 2016).

Debris flows are one kind of subaqueous sediment gravity flows, which are caused by excessive sediment density (Yang et al., 2019). They are defined as a laminar plastic flow in which sediment is supported by the matrix strength, grain-to-grain interactions, excess pore fluid pressure, or buoyancy (Talling et al., 2012; Yang et al., 2019). Although more detailed classifications exist, debris flows can be typically subdivided into two types: sandy (or noncohesive) debris flows, and muddy (or cohesive) debris flows (Shanmugam, 1996; Tallinget al., 2012; Shanmugam, 2000; Yang et al., 2019). More detailed description and classification about debris flows can be found in Talling et al. (2012).

Evaluation of downslope mass movements and investigation of slope stability of a region as well as their formation and triggering mechanisms draw attention in recent years since they are quite important for the risk analyses related to the possible natural disasters (Cauchon–Voyer et al., 2008). This is because they (i) reshape the continental slopes, (ii) directly affect the sedimentary structure of the slope and deep basins, (iii) carry large amounts of sediments to deep basins, (iv) have the potential to create destructive tsunamis, (v) may damage to offshore geoengineering structures such as pipelines or submarine cables, and (vi) constitute good cap rocks for deeper hydrocarbons due to their low permeability and porosity (e.g., von Huene et al., 2004; Krastel et al., 2006; Dondurur and Çifçi, 2007; Reece et al., 2012; Dondurur et al., 2013; Sun and Alves, 2020; Sun and Leslie, 2020). In addition, subaqueous sediment gravity flow deposits are considered as a major reservoir plays in lacustrine basins today (Yang et al. 2019).

Even though the morphology of Danube Delta system and the mud volcano area along the southern part of the Crimea in the Black Sea have been studied in detail, our knowledge on the morphological and sedimentological characteristics of the Turkish margin along the Black Sea is quite limited. This region has also become an interesting area for hydrocarbon exploration in relatively deep water zones for the last two decades (Robinson et al., 1996; Menlikli et al., 2009). In addition, the Black Sea hosts a number of deep-sea natural gas pipelines such as Blue Stream, Turkish Stream and South Stream. For these reasons, mapping the shallow sedimentary structure, sediment movements and unstable areas along the margin is important in terms of positioning and operating future engineering structures in the region. Also, understanding the triggering factors of submarine failures is important for hazard mitigation processes for coastal areas.

The purpose of the present study is to document the distribution and characteristics of the stacked debris flows observed in the Plio–Quaternary sediments along the continental rise of Sakarya Canyon using seismic data. The physical properties, sizes and run–out distances of the debris flows as well as areas affected by the debrites based on their characteristic appearance in the seismic data are also discussed. In addition, we investigate the different agents promoting the debris flows and possible triggering factors as well as their formation mechanisms.

2. Tectonic setting

The Black Sea is a large basin located at the north of the North Anatolian Fault (NAF) and on the western flank of the active Arab–Eurasian continental collision (Figure 1a). Although it is within the Alpine–Himalayan orogeny and is surrounded by compressive belts, it exhibits extensional tectonics in origin (Robinson et al., 1996). The Black Sea consists of two basins, the western (WBS) and eastern (EBS) basins, which are separated by the Mid Black Sea Ridge (MBSR) (Figure 1a). MBSR is subdivided into two parts as Andrusov Ridge to the north and Archangelsky Ridge to the south. According to many researchers, the Black Sea is a back-arc basin of the northwards subducting Tethys Ocean, behind the Pontid volcanic arc (Zonenshain and Le Pichon, 1986; Finetti et al., 1988; Robinson et al., 1996). WBS has an oceanic crust and the sediment thickness since opening from the Upper Cretaceous reaches 15 km in the center of the basin (Nikishin et al., 2015).

The Black Sea and its surroundings are defined as a region with low seismicity (Tarı et al., 2000), the most important seismicity is not related to the Black Sea itself but related to large regional faults such as NAF. The 1968 Bartın earthquake on the boundary of WBS is the strongest earthquake that was instrumentally recorded, and its source mechanism indicates thrust faulting (Alptekin et al., 1986).

The morphological features of the western Black Sea continental margin are similar to the characteristics of modern ocean margins. It consists of a narrow shelf, a steep continental slope, an apron (or continental rise) with a smooth bathymetric gradient and an almost flat abyssal plain extending northwards. Morphologically, the Black Sea shows two different types of margins, shelf has not developed along the eastern and southern borders. In these regions, the continental slope is quite steep, and approx. 1800 m water depths are reached just in 15 km northwards from the shelf break. On the other hand, along the northern and western borders, a considerably wide shelf and a lower gradient continental slope is observed.

The study area is located in the western Black Sea continental margin, where semi–confined meandering Sakarya Canyon exists offshore of the Sakarya River (Figure 1b). The shelf break in the area is located at about

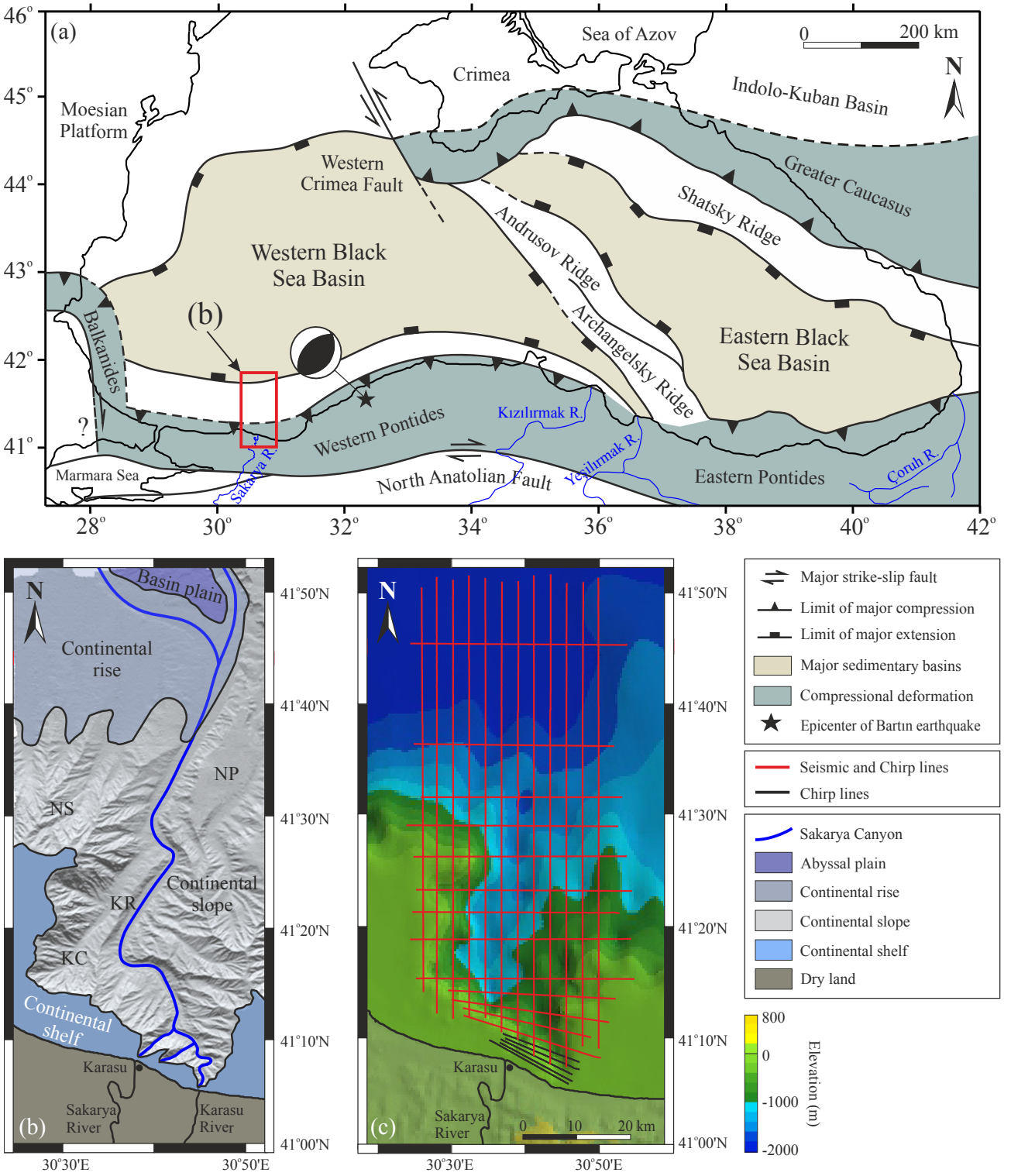

Figure 1. (a) Major tectonic elements of the Black Sea (modified from Finetti et al., 1988; Robinson et al., 1996). Location and fault plane solution of Bartın earthquake are from Tarı et al. (2000), (b) main morphological divisions and elements of the study area (KC: Kefken Canyon, NP: Northern Platform, KR: Kefken Ridge, NS: Northern Slope), and (c) the location of the collected seismic lines.

120 m isobath. The three heads of the Sakarya Canyon are located very close to the coastline, where the shelf platform in this area is not developed due to the canyon heads. The continental shelf on the western and eastern parts of the canyon are 8 and 14 km wide, respectively. Between the shelf break and about 1600 m water depths, there is a continental slope with a relatively high slope inclination (a maximum of about 25°). Further north, there exists the continental rise where the bathymetric gradient is relatively low (maximum 5°) and an almost horizontal abyssal plain (Figure 1b).

Studies on marine geology in this area are very limited. Algan et al. (2002) observed extensive normal faulting on single channel seismic sections collected from the shelf area. They suggested that these faults may be a strike-slip fault system that forms a flower structure as they tend to merge at deep in the sediments. In addition, in the deep part of the canyon, there are active faults in the NNE–SSW direction reaching to the sea floor (Yiğitbaş et al., 2004). Along the continental rise, Nasıf et al. (2020) showed that there are also areas of submarine fluid flow, shallow gas accumulations, gas chimneys, bottom simulating reflectors (BSRs) and mud volcanoes.

3. Data and methods

High resolution multichannel seismic reflection, Chirp subbottom profiler and multibeam bathymetric datasets were collected simultaneously onboard of K. Piri Reis research vessel operated by Dokuz Eylül University, Institute of Marine Sciences and Technology during the two separate cruises in 2012 and 2016 along the Sakarya Canyon. Figure 1c shows the locations of the lines acquired. A global DGPS system with a horizontal accuracy of approx. 0.5 m was used during the entire study. A total of approx. 1400 km of multichannel seismic reflection data was recorded using a 168 channel seismic recorder and a 1050 m digital streamer. Recording time and sampling interval were 6 s and 1 ms; source and streamer depths were 3 and 4 m, respectively. A generator-injector (GI) type air gun with a volume of 45 + 45 inc^3 was used as a seismic source, which suppresses its own bubble noise, and was fired at 25 m intervals. A conventional data processing flow was applied to the raw seismic data using SeisSpace Promax software. Data processing steps for multichannel seismic reflection data include data loading, geometry definition, band-pass filter (8–180 Hz), trace editing, f–k dip filter, suppression of multiples with surface-related multiple elimination (SRME) method, sorting to CDP gathers, velocity analysis (at about every 1000 CDPs), NMO correction, stacking, poststack time migration and gain application.

Multibeam bathymetric data was collected using a SeaBeam 1050D system with hull-mounted transducers. It is an equi-angle system which utilizes 126 beams at 50 kHz frequency and the total swath range is 153°. Bathymetric data was processed using Caraibes software with the following conventional data processing steps: data loading, beam editing and de–spiking, correction of the navigation errors, data interpolation, gridding with 100 m grid interval and digital terrain model (DTM) construction.

4. Results

4.1. Structure of the debris flows

Along the northern part of the study area, where a relatively smooth bathymetric gradient exists, we observed 14 buried debris flow lobes in the multichannel seismic sections in waters deeper than approx. 1600 m. These were named as DB1 to DB14 from west to east. Figure 2 shows the locations of these debris flows on the multibeam bathymetric map and 3D views of their upper surfaces from different viewpoints. In Figure 2, debris flows are shown in different color codes as the debrites in the western (red), middle (blue) and eastern (green) part of the area. The western boundaries of DB2, DB3, and DB6 flows exceed the limits of our study area, and therefore, the western border of these flows could not be mapped accurately.

The debris flows are lens-shaped structures in stacked form in the seismic sections, usually having the largest thickness in the middle part. The direction of almost all debris flows is from south to north (from the lower continental slope to the deep abyssal plain). In addition to these relatively large debris flows, traces of smaller debris flow structures in shallower depths in the sediments are also observed in seismic data, but they are not mapped here.

Table shows some geometric properties of the debris flows calculated from the seismic data. They are, as observed in the seismic data, given from west to east and are categorized in three groups according to their locations. Figure 3 shows a graphical comparison of the properties of buried debris flows given in Table. The depth of the head parts of the flows from the seabed varies between 25 and 736 ms (approx. 20–590 m for an average sediment velocity of 1600 m/s). All of the flows are inclined to the north, and their depth from the seabed increases regularly towards the deep basin. The depths of their northern edges range from 105 to 986 ms (approx. 84–790 m for an average sediment velocity of 1600 m/s). Their run-out distances change from 3.8 to 24.4 km. The third group in the far east of the area (the green group) are of the smallest sediment volumes with the shortest run-out distances. Seismic data indicate that the run-out distances of the stacked debris flows and the vertical distances between them are not systematic.

From the graphic shown in Figure 3a, DB3, DB4, and DB6 flows have the steepest inclination to the north. The

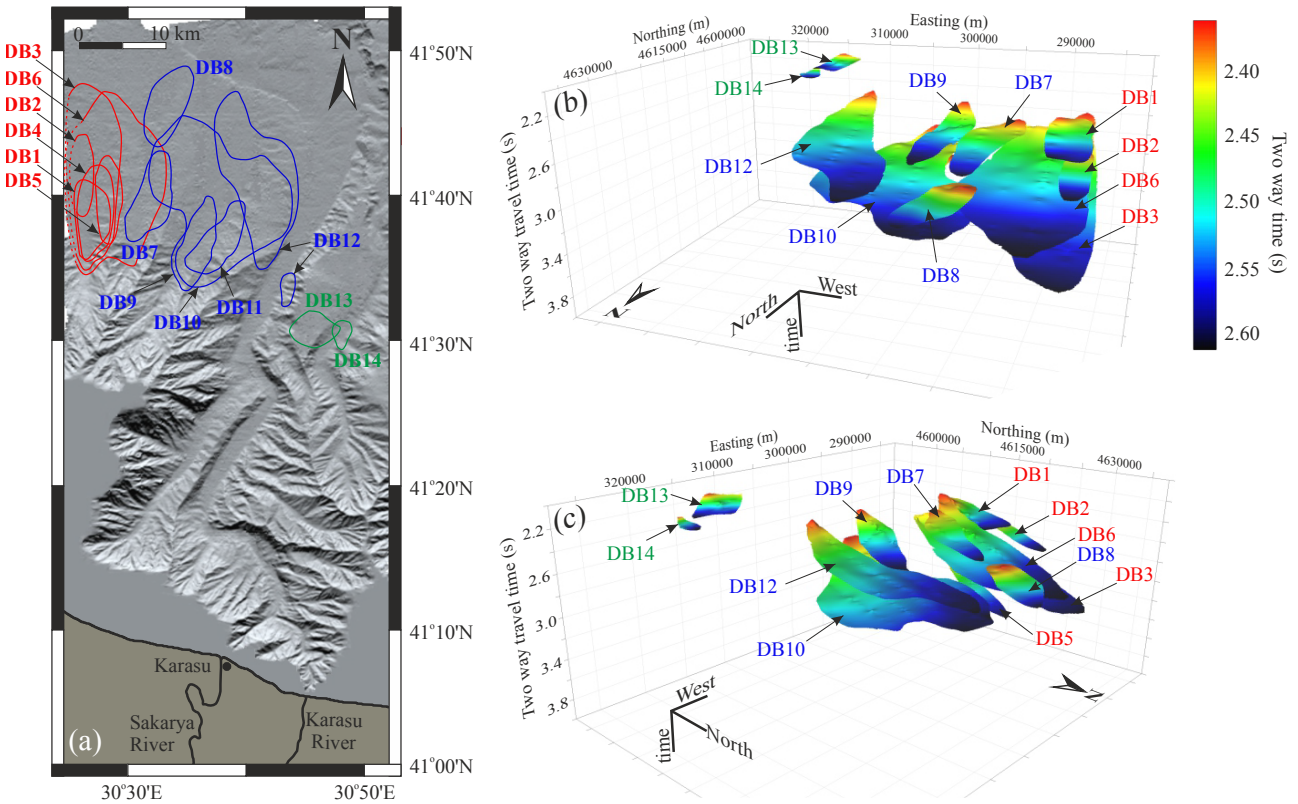

Figure 2. Locations of the debris flows along the continental rise. (a) On the multibeam bathymetric map, and 3D views of their upper surfaces (b) in NW and (c) in NE directions. It is not possible to show DB11 and DB4 in 3D views since they are buried under DB10 and DB3, respectively. Color codes of the debris flows are given according to the classification in Table. X, Y and t axes correspond to E–W, N–S, and time axes, respectively.

average thickness of the debris lobes is approx. 73 m, which generally increases as their burial depth increases (Figure 3b). DB10 has the largest volume and it is calculated that a total of 15.13 km^3 of sediment transported along this flow (Figure 3c), which also has the largest surficial area affecting a total area of 224.9 km^2 (Figure 3d).

The burial depths of the flow heads typically located at the southernmost parts of the flows are not proportional to the ages of the flows. This is because the flows are located in the continental rise of the study area, which is considered to be the main sediment accumulation zone. In this part, the Plio–Quaternary sediment thickness increases rapidly towards the north, but some of the flow heads have quite shallow burial depths because they are located close to the toe of the slope to the south. It is also observed in the seismic data that especially the heads of the first group debris flows (the red group in Figure 2 and Table) are founded upon the acoustic basement (Figure 4a). Figure 4a shows an example seismic section for this situation, in which we observe a number of stacked buried debris flows from the red group, whose depths from the seafloor increase rapidly towards the north. Although the head part of DB6 flow, for example, is located at a smaller burial depth than those of DB1 and DB2 flows, DB6 is older than DB1 and DB2 (Figure 4a).

Figure 4b shows a fence diagram prepared using 5 parallel seismic sections in the N–S direction and an E–W section that crosscuts them to illustrate the relationship of the debris flows in group 2 (the blue group in Figure 2 and Table). Since there are several debris flows in the stacked form in the area, it is important to accurately determine their lateral continuity using 2D seismic lines. This process can be done by jump correlation along the intersecting seismic profiles.

The appearance of flow structures on the seismic sections is quite distinct with respect to the surrounding sediments: Their internal structures are typically chaotic and/or transparent with almost no reflections of trace–

Table. Some geometric properties of the debris flows calculated from the seismic data. The depth conversion was done by using an average sediment velocity of 1600 m/s. The order and color codes of the debris flows are from west to east according to their locations in Figure 2a.

Group	Debris flow	Age[a]	Run-out distance (km)	Failure direction	Total volume (km^3)	Surficial area (km^2)	Maximum thickness[b] (m)	Depth of southern edge[c] (ms)	Depth of northern edge[c] (ms)
1	DB1	1	10.3	S–N	0.52	32	24	25	105
	DB2*	7	10.6	S–N	0.77	22.3	52	120	271
	DB3*	10	24.1	S–N	8.26	120.2	84	164	767
	DB4	11	12.5	S–N	2.80	42.9	88	296	728
	DB5	14	11.2	S–N	2.06	25.4	121.6	736	986
	DB6*	9	24.4	S–N	12.64	186	72	50	553
2	DB7	2	12.3	SSW–NNE	1.33	38.4	60.8	133	204
	DB8	6	11.2	SSW–NNE	1.31	38.3	52	269	288
	DB9	8	12.5	SSW–NNE	1.85	37.1	82.4	215	287
	DB10	12	22.4	S–N	15.13	224.9	109.6	484	650
	DB11	13	11.0	SW–NE	2.75	32.7	138.4	512	756
	DB12	5	23.3	S–N	4.68	121.4	53.6	122	243
3	DB13	3	4.6	GB–KD	0.75	18.2	50	146	217
	DB14	4	3.8	S–N	0.18	5.76	40	230	250

a: the youngest flow is shown by 1 while the oldest one is 14 depending on their burial depth; b: maximum thickness in the central part of the flow; c: depths from the seabed.
*: Since the western boundary of these flows could not be mapped, the transported sediment volumes and the surficial areas in the table indicate the minimum values; actual values are probably higher than these estimates.

by–trace consistency consistent with the surrounding sediments. Figure 5a shows DB9, DB10, and DB11 while Figure 5b illustrates DB13 and DB14 as examples for groups 2 (blue) and 3 (green) debris flows. The western edge of DB13 flow terminates against on a small-scale slide structure, and seismic data indicates that this flow also passes through the Sakarya Mud Volcano feeding channel.

The appearance of the flows in 2D seismic sections is generally lens-shaped and the thickest part is typically located in the middle of the flow with decreasing thickness towards the edges. In general, their maximum thicknesses increase as the flows deepen. This is also valid for the updip parts (southern edges) of the flows, and we do not observe clear headwall scarps around the southernmost parts of the debris flows in the seismic sections (Figure 5a). The bottom surfaces of the debris flows are unconformable with the underlying sediments and are typically expressed as a distinct erosional interface possibly due to the sediment truncation formed during the sliding phase. In many cases, the underlying Plio–Quaternary sediments inclined from the south to the north terminate with a toplap at the base of the flows (Figure 5).

The upper surface of the flow is sometimes reshaped as a result of the subsequent sedimentary processes following the flow. The seismic sections in Figure 6 show examples indicating well-developed sediment waves along the NW part of the study area. Bottom surfaces of the debris flows in this region generally do not show erosional characteristics and are seen to be conformable with the underlying unit. It is also observed that the upper surfaces of the debris flow lobes were reshaped by these sediment waves that developed following the flows. The southern boundary of DB12 in Figure 6a is limited by a fault surface. The fault is located beneath the crest of a local ridge structure that forms a steep morphology at the seafloor and separates both flanks of the ridge. DB1 and DB12 flows developed within the sediment waves and were reshaped during sediment wave formation afterwards (Figure 6).

4.2. Effect of Sakarya Canyon

The most distinct morphological structure in the study area is the Sakarya Canyon. Sediment erosion on the continental slope and erosional truncations along the canyon walls show that the canyon is active in terms of sediment transport and erosional processes. Typically, the

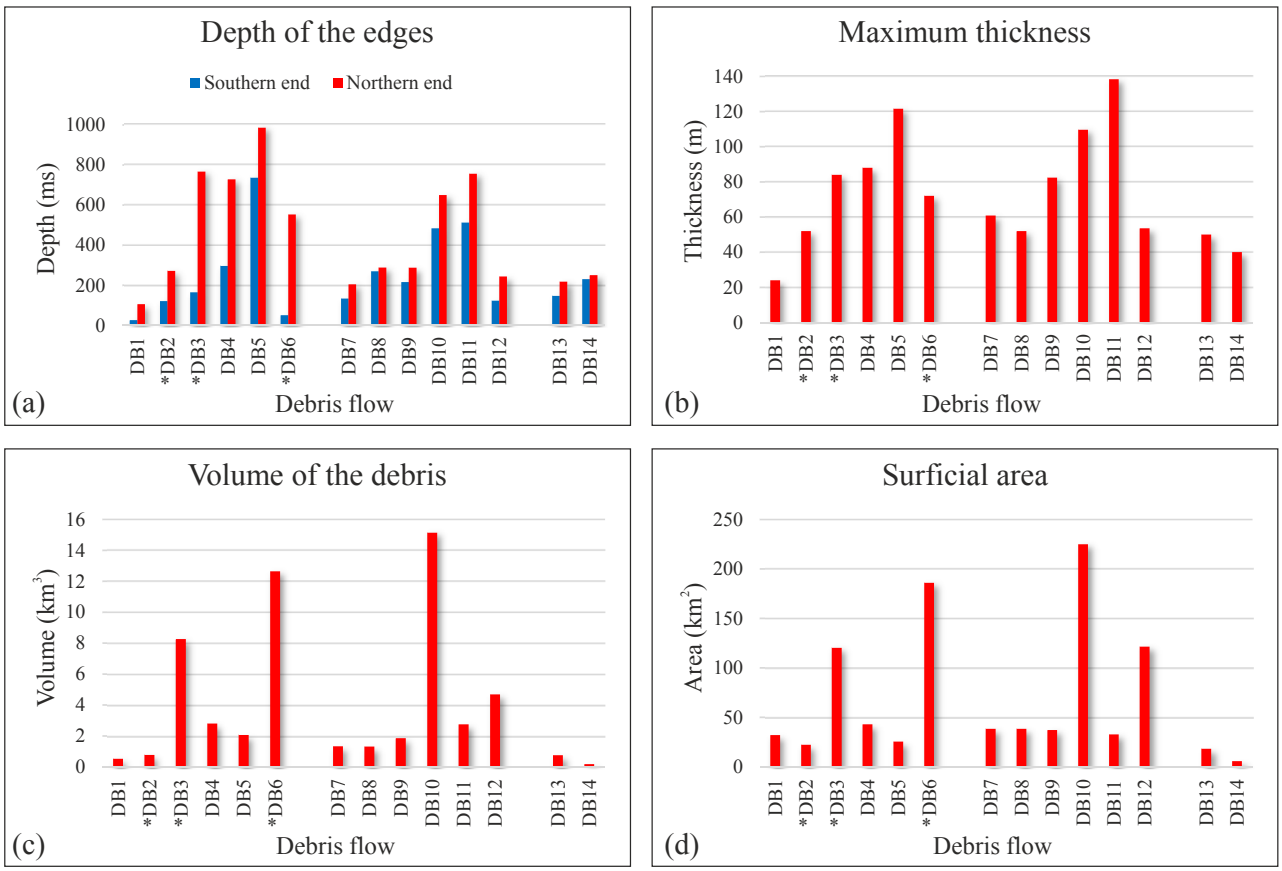

Figure 3. Graphical comparison of the features of buried debris flows given in Table. (a) Depths of the southern and northern edges of the flows from the seabed, (b) maximum thickness of each debris flow deposits, (c) total volume of the transported material, and (d) the surficial area affected by the debris flows. Since the western boundary of the DB2, DB3, and DB6 flows (signed with an *) could not be mapped, the sliding material volume and surficial area values show minimum values.

canyon exhibits a narrow and V-shaped crosssection in the southern parts close to the land, while its base expands to form a U-shaped structure in the deeper waters further north. The axis of the canyon is expressed by a very strong reflection extending almost horizontally in the seismic sections especially in the distal zone (Figure 7). Generally, a thin layer of turbidite accumulation is observed along the distal canyon axis over a distinctive erosional basal surface (Figure 7a). In the seismic section given in Figure 7a, the sediment erosion along the canyon floor is quite evident on DB12. In Figures 7b and 7c, two seismic lines perpendicular to this flow along with the seafloor bathymetry is shown from two different perspectives. The Sakarya Canyon axis appears as a prominent channel on bathymetric data, and the erosion of the DB12 flow over the canyon wall and axis can be observed from seismic data.

In Figure 7a, the seismic data indicates the sediments forming a local anticline by bending upwards due to the small-scale ridge structure located under the canyon axis. The tip of this anticline reaches to the base of the Sakarya Canyon, however, it is observed that this part of the anticline was completely eroded by sediment erosion along the canyon axis. This erosional process also affects buried debris flows such as DB12 in Figure 7. Even though it is of two pieces now, DB12 was a single piece debris lobe through the Sakarya Canyon axis when it was formed. However, the part of DB12 flow lying over the ridge structure and below the canyon axis has been completely eroded today due to the effective erosional process along the canyon axis.

4.3. Relations with submarine fluid flow

Extensive bottom simulating reflectors (BSRs), which indicate the base of gas hydrate accumulations, have been

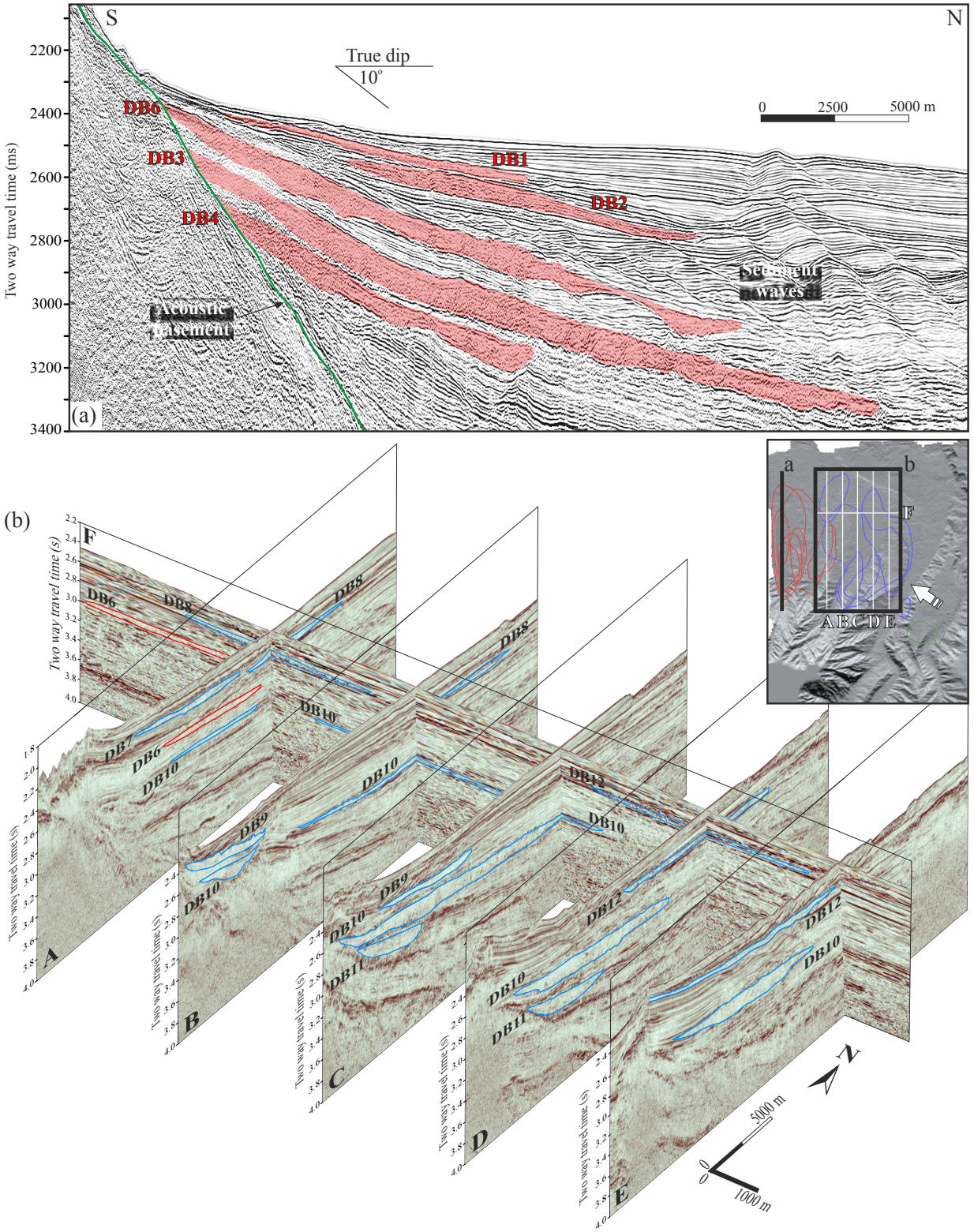

Figure 4. (a) Seismic section extending in N–S direction in the NW part of the study area consisting of several stacked debris flows, and (b) fence diagram composed of seismic sections particularly including group 2 (blue polygons in Figure 2) debris flows. The white lines on the location map correspond to the seismic sections indicated by A to E. The white arrow shows the view direction of the fence diagram.

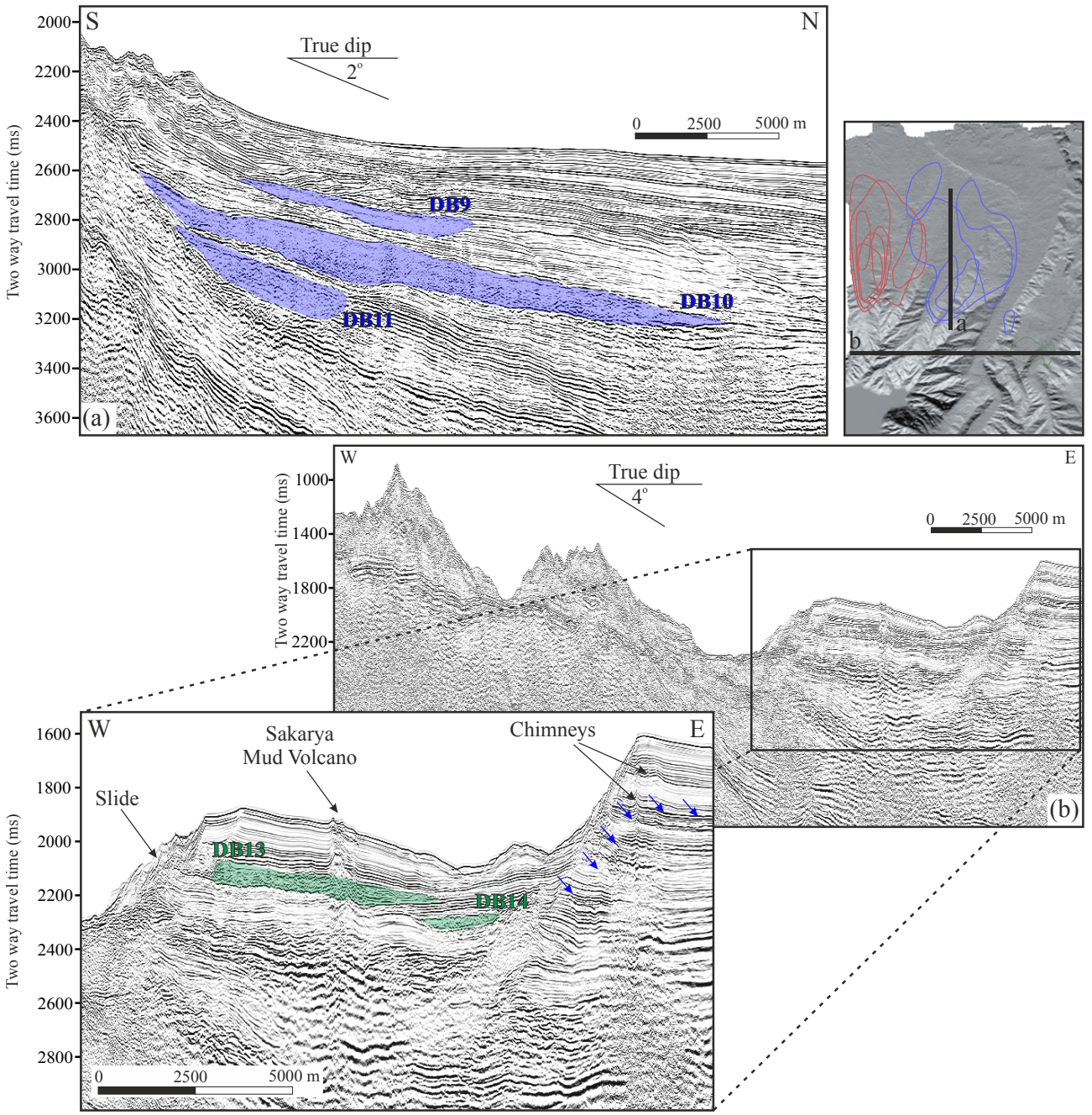

Figure 5. Seismic sections for debris flows showing (a) DB9, DB10, and DB11, and (b) DB13 and DB14 flows. Debris flows are distinguished by their transparent internal structures, lens-shaped appearances and erosional lower and upper surfaces. Blue arrows locate the BSR reflection.

observed in the area. The depths of BSRs from the seabed are between 70 and 350 ms increasing towards the north. Figure 8a shows the distribution of BSRs and their depths from the seafloor, superimposed on the map showing the locations of some debris flows which are located within the underlying sediments of the BSRs (DB3, DB4, DB6, DB9, DB10, and DB11 flows). According to this BSR distribution map, it is observed that there is no BSR within the sediments overlying the debris flows if the flows are deeper in the sediments than BSRs, especially in the region

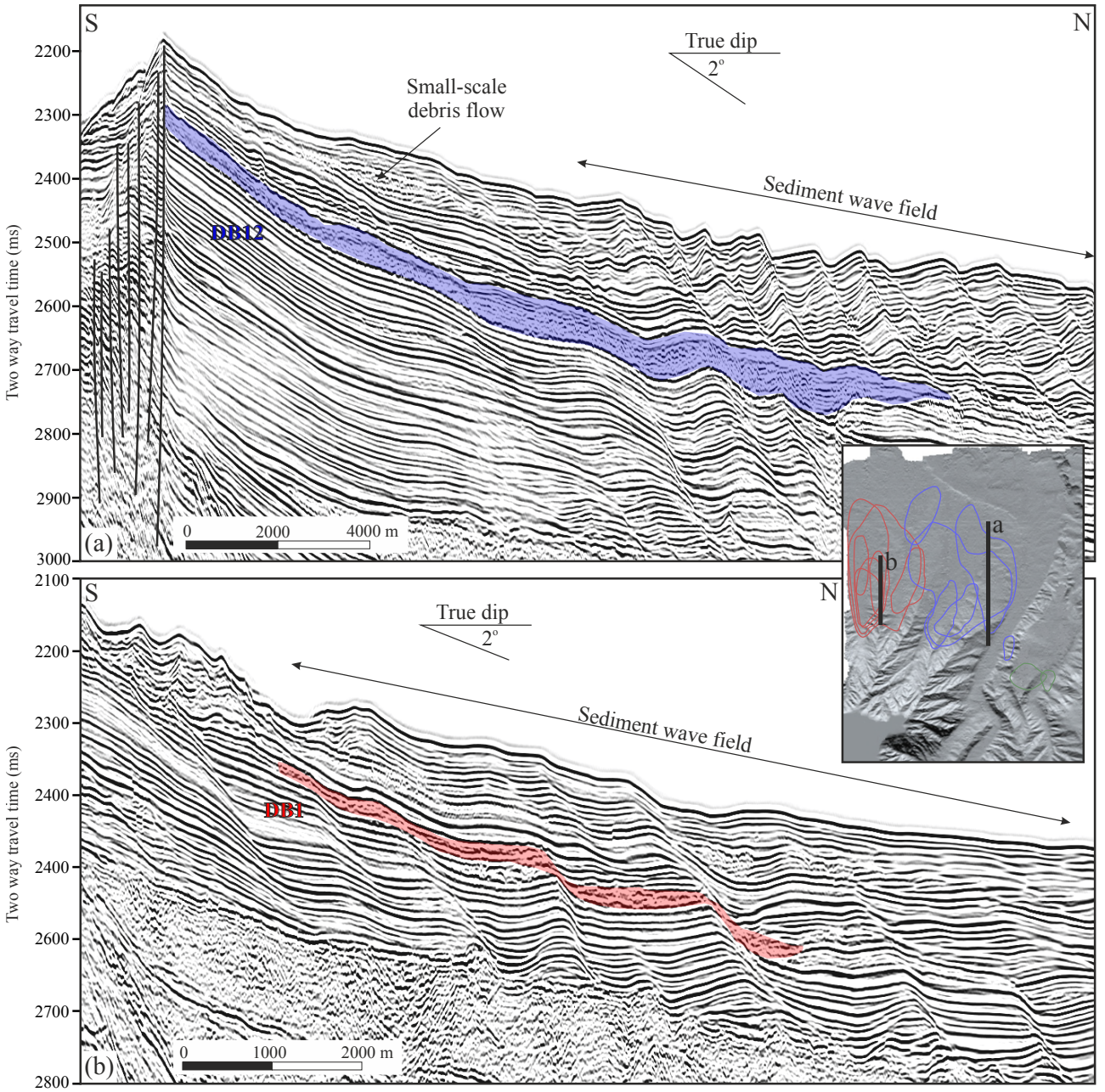

Figure 6. Seismic sections showing (a) DB12 and (b) DB1 debris flows reshaped by sediment waves in the NW part of the area.

where the second group of debris flows (the blue group in Figure 2 and Table) are located. This situation is also clear in 3D representation given in Figure 8b. Figure 9 shows two example seismic sections for this situation. If there is a debris flow accumulation in deeper sediments, then the BSR reflections in shallower sediments appear in areas where debris flow accumulations laterally terminate. In other words, if there is one or more debris lobes in the underlying sediments, then there is no BSRs, and hence gas hydrate formations, over these lobes in the shallower part of the sedimentary column [except DB6 debris flow, along the eastern part of which we observe a BSR (Figure 8a)]. On the other hand, this does not apply to the debris flows located within the shallow sediments overlying the BSRs. That is to say, a debris flow accumulation located at shallower depths than BSR depths has no effect on BSR formation (e.g., DB12 debris flow in Figure 9b).

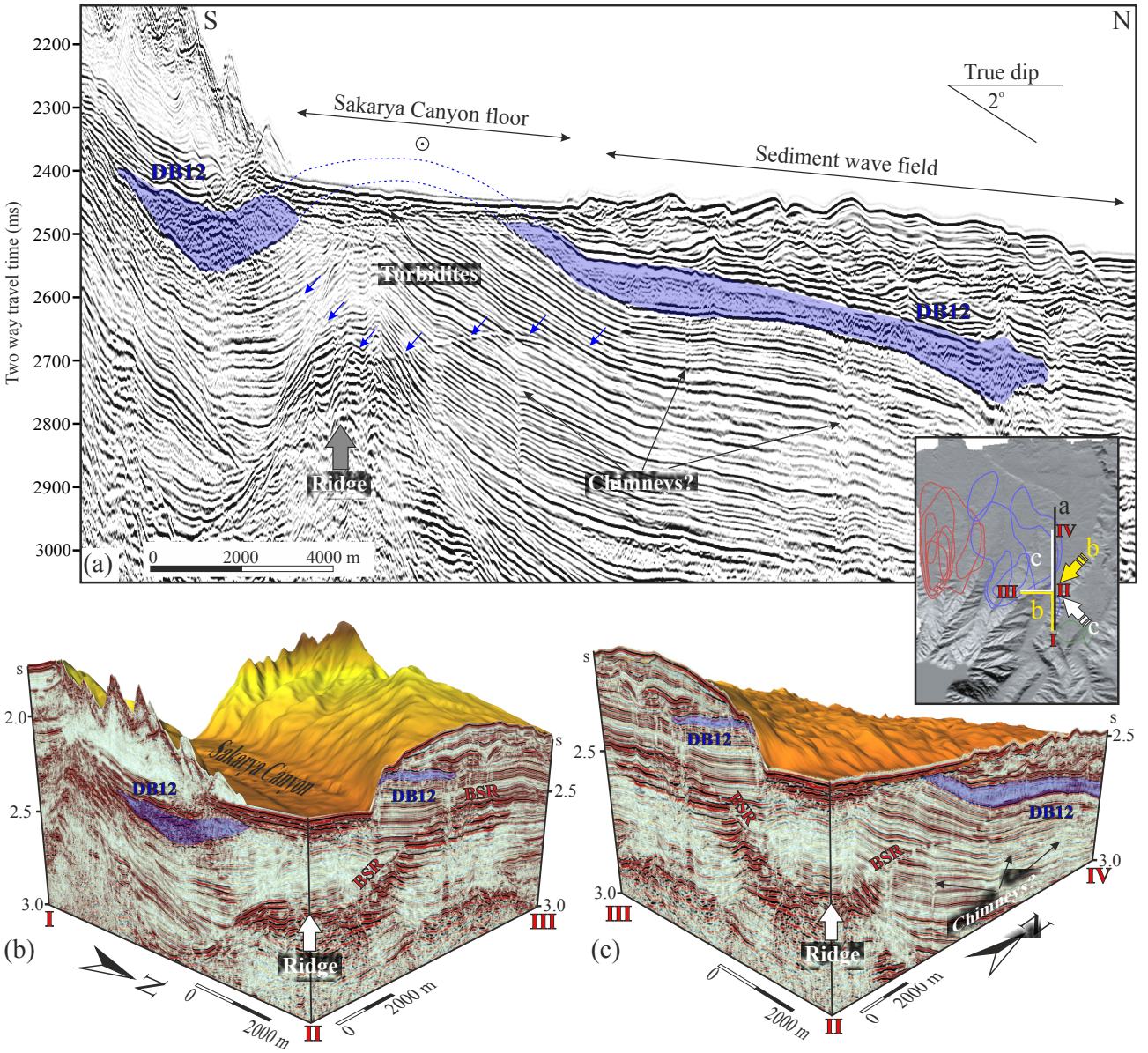

Figure 7. Effect of sediment erosion on the debris flows along the Sakarya Canyon axis. (a) Erosion of DB12 flow in a N–S extending seismic section which obliquely crosscuts the canyon axis, (b) and (c) views of the same flow in two intersecting seismic sections with two different perspectives from NE and SE directions, respectively. The blue dashed line corresponds to predicted part of DB12 eroded by canyon floor erosion. Yellow and white arrows indicate the view directions for the 3D visualizations in (b) and (c), respectively. Blue arrows locate the BSR reflection in (a).

5. Discussion

5.1. Sedimentation and source area

The onshore part of the study area is the western Pontides belt named as İstanbul Zone (Okay et al., 1994). This region is the catchment area of the terrigenous sediments while the main sediment deposition region is the continental rise area. The topography, size, sediment type and cementation of the sediments in the source area as well as the climatic conditions prevailing in this region widely affect the type and amount of the sediments in the deposition (or sink) area.

There are two major rivers on the land of the study area: the Karasu River to the east and the larger Sakarya River (Figure 1b). Both rivers flow along the Adapazarı plain

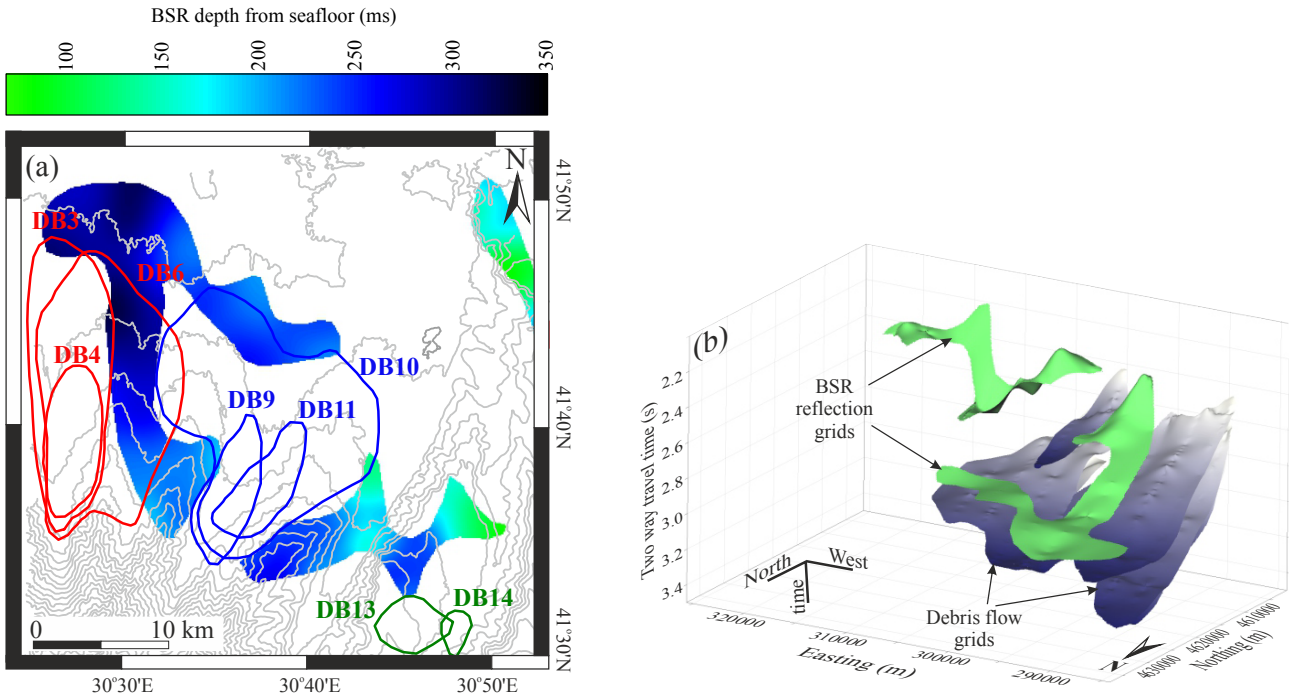

Figure 8. (a) Distribution and depth map of the BSR reflections in the study area and the location of the debris flows lying beneath the BSRs (DB3, DB4, DB6, DB9, DB10, and DB11 flows) superimposed on the depth contours of the area, (b) 3D view of the map in (a). Except for the eastern part of DB6 flow, no BSR reflection is observed in the shallow sediments overlying the debris flows. See text for details.

and constitute the most important transport pathways for the terrigenous sediments to be transported to the sea. The discharge rate of the Sakarya River is around 5.6 km^3/year being 14% of all large Anatolian rivers (Algan et al., 2002) such as Kızılırmak, Yeşilırmak and Çoruh in the eastern Black Sea. The drainage basin of the river is generally composed of Eocene flysch deposits, Upper Cretaceous limestones and Devonian schist (Algan et al., 2002; Yiğitbaş et al., 2004). There are terrigenous Pliocene deposits and Quaternary alluvium along the coastal area.

Due to the high amount of agricultural activities and low vegetation in the south, the sediment load carried by the Sakarya River is quite high. The annual average sediment load is ca. 3.8 million tons/year constituting 16% of the sediment amount transported from all Anatolian rivers (Algan et al., 2002), which discharge the terrigenous sediments directly into the narrow shelf area offshore. However, Sakarya River discharges its main sediment load to Adapazarı plain before reaching the sea. Bilgin (1984) suggested that, following the construction of 11 large dams along the Sakarya River in the last 2 decades, the coarse grained material carried by the Sakarya River accumulates in the Adapazarı plain, while the finer grained sediments is transported to the sea.

Late Pleistocene–Holocene stratigraphy of the Black Sea typically show three distinctive sedimentary units. When the Black Sea was a fresh water lake during the Last Glacial Maximum, a lacustrine clay unit (Unit 3), so called Lutine unit, deposited. After the connection with the Mediterranean at 7150 years BP, a finely laminated sapropel unit (Unit 2) of ca. 40 cm thick deposited due to a high organic productivity and limited circulation. Following the establishment of the present-day oceanographic conditions, an approx. 30 cm thick coccolith unit (Unit 1) started deposition in the deep basin (Çağatay, 1999; Akyüz et al., 2001). Gravity cores collected from the upper continental slope of the western Black Sea clearly show this sedimentary succession (Duman, 1994; Genov, 2009), if there is no bottom current activity to modify or disturb the original sediment deposition.

Sakarya Canyon, along with the Kefken Canyon further west (Figure 1b), is the most prominent morphological structure in the study area, and it is suggested that it has significant effects on deep sea sedimentation in the area

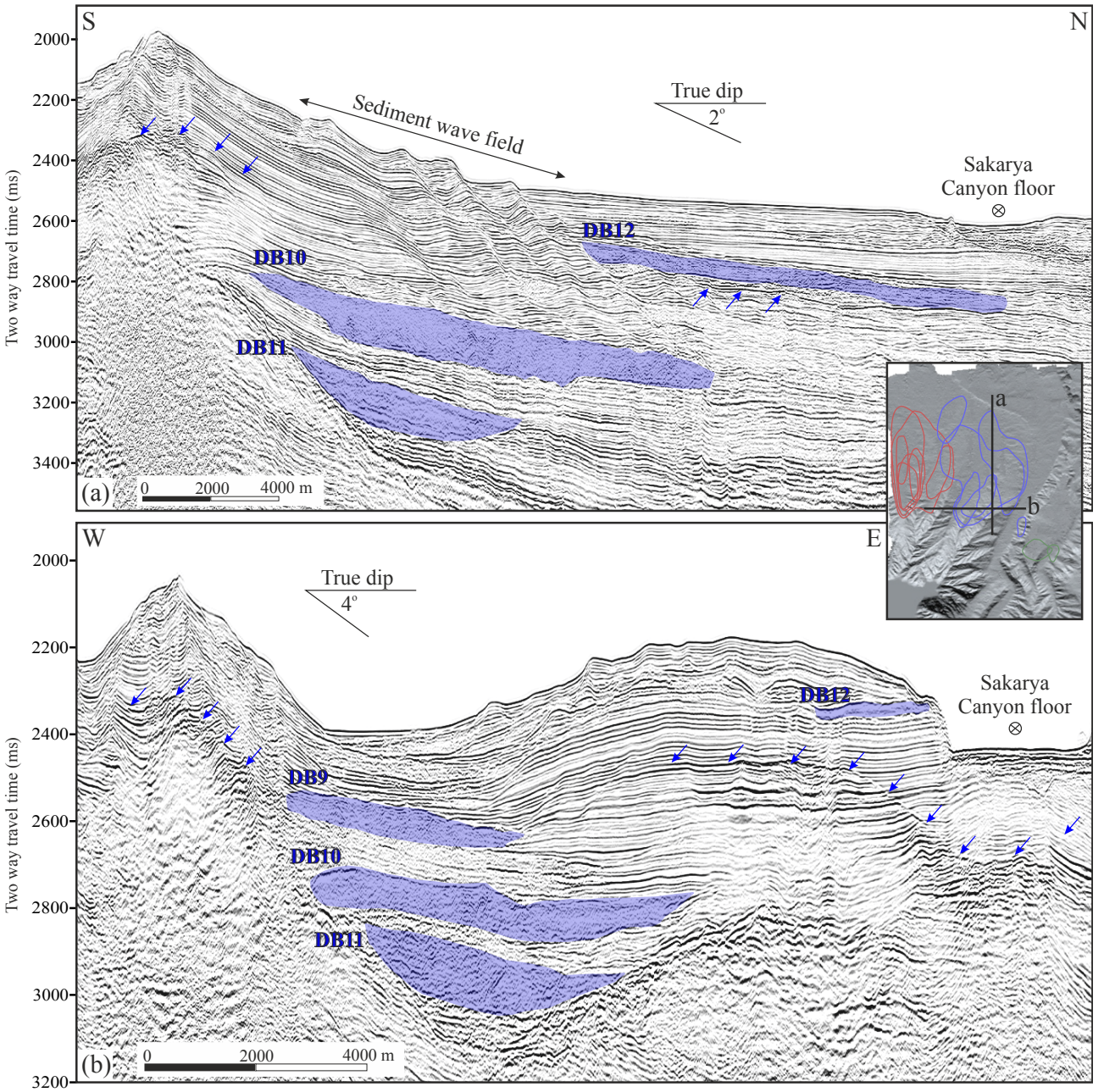

Figure 9. Seismic sections indicating the relationship between BSR reflections and debris flows. (a) N–S and (b) E–W extending seismic sections with BSRs and stacked debris lobes. Blue arrows locate the BSR reflections. In general, no BSR reflection is observed in the sediments overlying the debris flows. See text for details.

(Nasıf and Dondurur, 2017; Nasıf et al., 2019, 2020). The canyon is located at the mouth of the Sakarya River and extends from shelf break to deep abyssal plain. Nasıf et al. (2019) proposed that the main sediment deposition types along the continental rise in waters deeper than 1500 m are turbidites interbedded with pelagic/hemipelagic sediments. Duman (1994) defined thick (from 3.6 to 10.4 cm thickness) turbidite layers alternating with coccolith layers on two gravity cores taken from the continental rise.

There is no detailed description of the deep-sea sedimentation in the study area defining the composition, amount and contents of the sediments in the continental

rise where we observe debris flows. We tentatively suggest that terrigenous sediments are sourced from Adapazarı basin on land and they are transported to the coastal area by Karasu and Sakarya Rivers (Figure 1a). This terrigenous sediment input is then transported from shallow shelf to the deep basin by different ways such as turbidity current activity along the Sakarya Canyon system, slumps, slides as well as debris flows to constitute deep water sediments interbedded with pelagic/hemipelagic sediments.

5.2. Structure of the debris flows

Debris flows observed in the region are interpreted as gravity flows formed in areas close to the region where Sakarya Canyon reaches to the abyssal plain in the north (Figure 2a). The flows are all buried and the seismic and Chirp subbottom profiler data indicate that there is no recent debris flow located on the seafloor, or their sizes are beyond the resolution limits of our dataset. The shallowest one mapped by the seismic data is DB1 which is located at a depth of approx. 20 m from the seafloor (Table). Although there are no debris flows onto the seafloor, the stacked structures of the flows in the region indicate that the sliding in debris flow form is an ongoing process in this area.

The reflections from the upper and bottom surfaces of the debris flows generally indicate that they are in erosional form which is unconformable with the underlying stratigraphic units (Figures 4a and 5a). The erosional base is probably associated with the erosional truncation occurred during the flowing process, and the erosive upper surface is related with the irregular accumulation of the postflow material. The debris lobes show almost no internal reflections possibly due to an irregular deposition of the unconsolidated material during the failure. Several buried debris flow structures have been defined on the seismic data in different regions of the Black Sea (Dondurur et al., 2013; Atgın et al., 2014; Tarı et al., 2015; Sipahioğlu and Batı, 2017; Hillman et al., 2018) with similar characteristics such as the absence of headwall scarps, erosive appearance of top and bottom surfaces as well as transparent internal facies.

The sizes of the debris flows observed in our study area as well as their structure and appearance on the seismic sections are quite similar with those observed in the world ocean margins. For example, run-out distances of debris flows observed in Austrian Molasse Basin vary between 3.8 and 15.5 km, and the total volume of the transported material is between 1 and 29.6 km^3 (Kremer et al., 2018). Rovere et al. (2014) reported 7.8–13.2 km run-out distances for the debris lobes observed in the NE Sicily margin, and the total affected surficial area was between 9 and 63.2 km^2. A similar study has been done by Dondurur et al. (2013) for the Amasra Bank, approx. 80 km east of our study area, and the run-out distances of several debris flows in this region are calculated as 9.6–24.8 km, the affected surficial areas are 23.8–263.5 km^2 with a total volume of sliding material as 0.4–12.2 km^3. Although these flows are structurally similar to those observed in our study area, the debrites offshore Sakarya River are in stacked form. This indicates that the flows in the area have occurred periodically over time, and this part of the region in the past was quite unstable due to the ongoing sliding processes. The sediment thickness (ranging from 8 to 150 m, decreasing westwards) between the stacked debris flows indicates that the time period between the formation of the flows maybe in between 26 and 500 ka considering a 30 cm/ka of average sedimentation rate (Ross, 1977).

None of the buried debris flows in the study area has a clear headwall scarp. Generally headwall scarps are observed in the seismic data at the upper parts of the recent slumps and slides on the seafloor (e.g., Antobreh and Krastel, 2007; Rovere et al., 2014; Çukur et al., 2016), but it is typically not possible to define the headwall scarps for buried debris flows (e.g., Diviacco et al., 2006; Wilken and Mienert, 2006; Dondurur et al., 2013; Kenning and Mann, 2020; Kret et al., 2020). The reason why the debrites in the study area could not be associated with a distinct headwall scarp could be because the flows have been displaced far from their source areas due to their relatively large run-out distances. A similar interpretation has also been suggested by Ducassou et al. (2013) for Nile deep sea fan. In addition, the heads of the debris flows, especially in the western part of the study area, are founded on the crystalline basement (Figure 4a). The inclination of the basement in this part is approx. 6.5°, and it is concluded that the source part of the debris flows may be located in the upper slope parts (more southern side) of the acoustic basement.

5.3. Triggering factors for the debris flows

There are many different agents that trigger submarine mass failures. These include seismicity or seismic loading, slope oversteepening, sea-level variations, local fault activity, submarine fluid-flow/gas hydrate dissociation, high sedimentation rates causing excess pore pressures as well as submarine erosional processes (e.g., Cauchon–Voyer et al., 2008; Mulder et al., 2009; Dondurur et al., 2013; Ducassou et al., 2013; Rovere et al., 2014; Çukur et al., 2016; Sun and Alves, 2020). Although the earthquake loading is considered to be the most effective factor for the mass movements, in most cases, multiple factors are effective on the failures.

5.3.1. Oversteepening of the slope

Western Black Sea continental margin offshore Sakarya River has relatively high slope gradients with inclinations exceeding 25° (Nasıf et al., 2020), which is possibly due to the Pontides thrust belt causing the oversteepening of the continental slope (Dondurur and Çifçi, 2007; Dondurur et al., 2013). The presence of a large number of block-

type sliding on the steep continental slope was observed in the seismic sections (Nasıf and Dondurur, 2017; Nasıf et al., 2019). However, the continental rise area where debris flows are observed has a relatively low bathymetric gradient (Figures 4a, 5a and 6) and the seabed inclination typically does not exceed 2°. This situation indicates that the oversteepening is not the primary agent promoting the debris flows in the continental rise while it could be considered as an important factor for relatively small-scale sliding along the steep continental slope due to the gravitational loading (Nasıf et al., 2019).

5.3.2. Local faults, structural effects and earthquake loading

Many researchers consider the seismic loading as the main triggering mechanism for submarine landslides (e.g., Evans et al., 1996; Lee and Baraza, 1999; Baraza et al., 1999; Bøe et al., 2000; Casas et al., 2003; von Huene et al., 2004). Observed debris flows are located close to the extensional deformation border of the western Black Sea basin (Figure 1a), however, extensional tectonics within the Black Sea is inactive today. The most important tectonic activity around the study area is related to the compressional tectonism of the Pontides thrust belt to the south close to the shoreline and the North Anatolian Fault (NAF) located ca. 140 km south of the continental rise of the study area (see Figure 1a for the location of NAF). The compressional tectonism of the Pontides thrust belt seems to be active since a moderate-size earthquake (M_S = 6.6) occurred in 1968 offshore of Bartın city, ca. 160 km east to the study area with a thrust faulting source mechanism (Alptekin et al., 1986). NAF, on the other hand, is a right–lateral strike slip fault which is quite active today and produces large destructive earthquakes along the northern Anatolia. It can be considered that effective seismic activity of NAF can be responsible for the different types of sliding along the whole margin including the debris flows in the study area.

In addition to the effects of the regional tectonism, using regional deep seismic reflection data, Yiğitbaş et al. (2004) reported NE–SW trending active normal faults lying parallel to each other with hanging–wall side towards the NW along the continental rise. They also mapped NNE–SSW trending strike-slip Adapazarı–Karasu transfer fault zone on the land within the Adapazarı basin to the south, which is proposed to be active producing seismic activity. In our seismic lines, we also observe active faults (not mapped here) along the distal parts of the Sakarya Canyon (see Figure 6a). The small-scale buried ridge structure in Figure 7 also indicates the structural activity within the region. The ridge is located just beneath the Sakarya Canyon floor and the sediments at both sides of the ridge onlap the ridge flanks (Figure 7a). They are also concave upwards at the ridge flanks, and the edges of DB12 around the tip of the ridge also bends upwards, which indicates the upward movement of the ridge is an ongoing process and uplifting continues after the failure of DB12. The local faulting in the region may also act as pathways for the submarine fluid flow to shallower subsurface depths forming local chimneys (Figures 5b and 7). Although we do not have reliable microearthquake activity data for the region, faults and the structural elements observed on the seismic profiles indicate that the local seismic activity may also play a secondary role on the formation of the debris flows, which may also be an agent for the triggering of the debris flows.

5.3.3. Submarine fluid flow and gas hydrate dissociation

Submarine fluid flow in the form of shallow gas accumulations and gas chimneys as well as dissociation of gas hydrates may promote submarine sediment failures. The gas in the shallow sediments can either be biogenic or thermogenic in origin, or provided by decomposition of gas hydrates. In any case, existence of gas in the pore spaces may result in excess pore pressures since the amount of existing gas is far beyond the solubility of the dissolved gas form in the aqueous solution. Grozic (2010) indicated that the failure occurs if the base of gas hydrate stability zone (BSR on the seismic data) and slide scars intersect, which makes the BSRs a potential geohazard.

Nasıf et al. (2020) mapped the BSRs, shallow gas, gas chimneys as well as mud volcanoes along the Sakarya Canyon and showed widespread gas hydrate occurrences along the western part of the distal Sakarya Canyon, which coincides with the area where we observe the debris flows (Figure 8). Although they do not know the exact composition of the gas within the shallow sediments as well as forming the gas hydrates, they proposed that the gas could contain thermogenic component because of the existence of deep-rooted gas chimneys and from the analysis of the thermobaric stability curves for gas hydrates.

Our seismic data show distinct BSRs around the debris flows in the area (e.g., Figures 5b, 7 and 9). In most cases, there is no BSR in the shallower sediments if there is a debris flow beneath (Figure 9). Several researchers (e.g., Dugan, 2012; Reece et al., 2012; Hornbach et al., 2015; Sun et al., 2018; Sun and Alves, 2020) suggested that the debrites can be characterized by their high velocity, bulk density and shear strength as well as their lower porosity, water content and permeability as compared to the surrounding sediments because of the overconsolidation of the debris material formed during their emplacement and burial. They also proposed that debris flow deposits can be considered as good seal units to prevent the vertical fluid migration after their emplacement. We, therefore, conclude that the debrites act as cap rocks for the fluids ascending from deeper sources, which also prevents the

formation of gas hydrates (and hence BSR reflections) within the sediments overlying the debris flows. That the gas chimneys from deeper sediments terminate at the base of the debris flows (Figure 7) also supports this interpretation. The only exception for this hypothesis is a part of DB6 debris flow (Figure 8a), some part of which is located directly beneath a BSR reflection. We tentatively interpret that the gas hydrates occurring directly above DB6 in this area might be formed by in situ biogenic gas production, or there would be a lateral gas migration especially along fractured basal shear of the debris as suggested by Sun and Alves (2020). In fact, this suggestion needs further investigation, especially applying gas chromatography analyses.

Seismic data show that the gas hydrates and debris flows coexist in the area. For offshore Amasra further east, Dondurur et al. (2013) suggested that gas hydrate dissociations are responsible for relatively large amphitheater-shaped submarine slides. They associated the gas hydrate dissociations with the sea level variations and a temperature increase within the water column due to the warmer Mediterranean Sea input following the rapid transgression period between 8500 and 7150 years before present as well as in the sediments due to the high sedimentation rate. In our study area, we do not know the exact timing of the debris flows, and therefore, we cannot provide a connection between the sea level rise in the Black Sea during Last Glacial Maximum (LGM) and the onset of the debris flows. However, considering the stacked form (Figures 4a, 5a and 9) and relatively large subsurface depths (Table) of the debrites in the area, they cannot be linked with the gas hydrate dissociations during a single sea level variation phase. In addition, we do not observe distinct acoustic turbidity zones below the base of the debrites or beneath the BSR reflections, which may indicate free gas accumulations in these zones. Therefore, we do not suggest that the submarine fluid flow has a primary effect on the initiation of the debris flows offshore Sakarya River.

5.3.4. Excess pore pressures due to high sedimentation

Debris flows are mainly located in the western region of the distal part of Sakarya Canyon (Figure 2a). This region is considered to be the deposition area along the continental rise and is not affected by the erosive effects of the canyon. Seismic data indicate that there is a thick Plio–Quaternary sediment accumulation in this region (Finetti et al., 1988; Nikishin et al., 2015), which inclined to the north with a structural inclination of ca. 2.2° (Figures 4a, 5a and 6). For this region, Ross (1977) and Çağatay (1999) proposed a sedimentation rate of >30 cm/ka while Duman (1994) suggested >100 cm/ka sedimentation rate. The burial depths of northern edges of the debrites are higher than those of southern edges (Table), which indicates that the sedimentation rate increases to the north towards the abyssal depths. The fact that the sediment packages surrounding the debris flows terminate with onlaps onto the highly inclined basement to the south (Figure 4a), and the increasing thickness of these packages inclined basinwards towards the north (Figure 5a) also supports this interpretation.

Atgın et al. (2014) reported large (reaching 500 m thickness around the continental rise) buried debris flows affecting a surficial area of 3500 km^2 along the Danube deep sea fan at the NW Black Sea, where high sedimentation rates exist (between 1.19 and 2.19 m/ka as an average, Winguth et al., 2000). Similar but smaller debris flows are also observed in the different parts of the Black Sea, especially in areas with high sedimentation rate and low bathymetric gradient (Dondurur et al., 2013; Tarı et al., 2015; Sipahioğlu and Batı, 2017; Hillman et al., 2018), which indicates that especially high sedimentation rates have an important effect on the formation of the debris flows. Excess pore pressures due to the high sedimentation rates sometimes cause massive submarine slope failures (Sultan et al., 2004; Talling et al., 2012; Dondurur et al., 2013) whenever pore pressures in fine-grained sediments exceed the confining pressure. We hereby suggest that the high sedimentation rate in the area where we observe stacked debris flows causes excess pore pressures within the underconsolidated shallow weak layers, which is the primary triggering factor for the debris flows.

5.4. A conceptual model for the formation of stacked debris flows

From the analysis of seismic data, a simple conceptual model consisting of four stages was developed to show the formation mechanism of the stacked debris flows in the region (Figure 10). According to this model, high sedimentation rate in the continental rise results in overpressure within the pore fluids of the unconsolidated subbottom sediments in stage 1 (Figure 10a). Both pelagic/hemipelagic sediments and turbidites contribute this high rate of sedimentation. In stage 2, a debris flow occurs at the seafloor due to the effect of the overpressured pore fluids with a possible triggering of the seismic activity of NAF and/or other local faulting. At this stage, the base of the debris flow might be coherent with the upper surface of the underlying sediment waves (Figure 10b). As the sedimentation continues, the debris flow formed in the second stage becomes buried and an overpressured zone develops again within the unconsolidated shallow sediments in the third stage (Figure 10c). At this stage, the inclination and the thickness of the sediment packages lying above the acoustic basement increases due to the basinal subsidence. That the inclinations of the layers are higher for deeper sediments indicates that the basinal subsidence is an ongoing process in this area. In the last

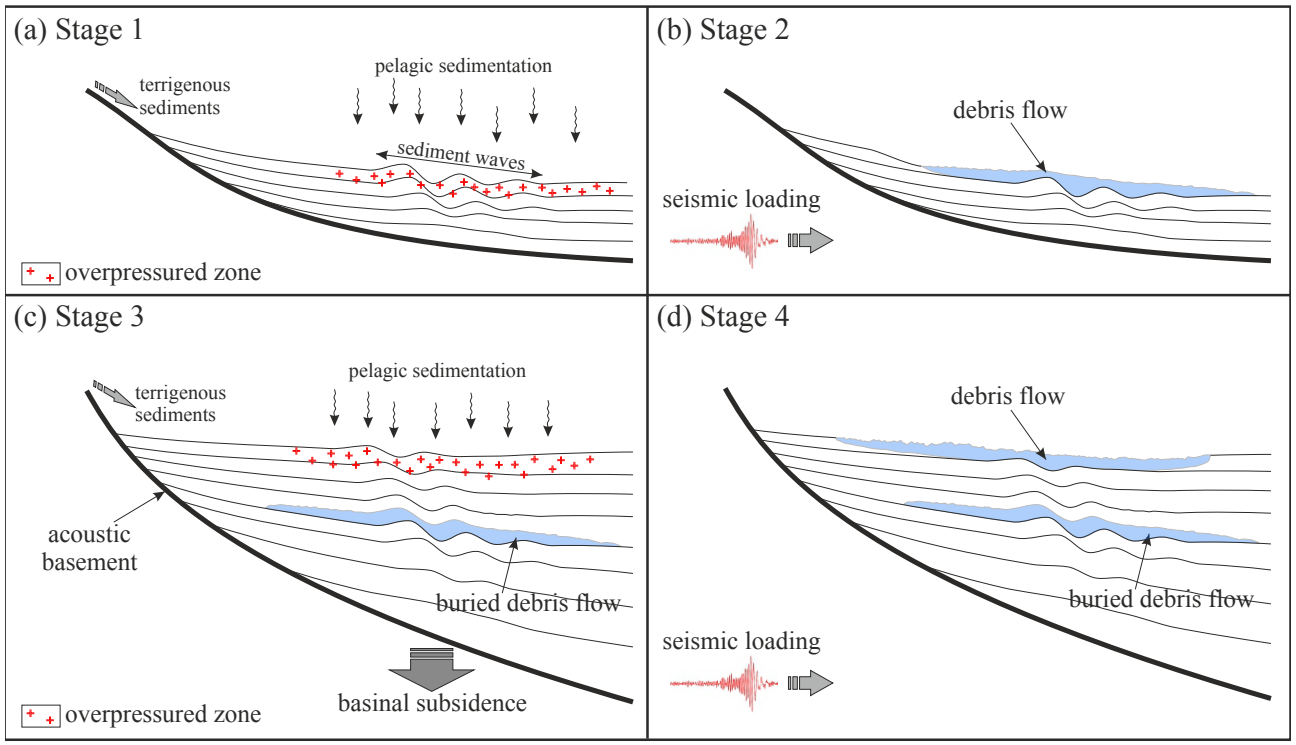

Figure 10. Conceptual model for the formation of stacked debris flows in the study area. (a) In stage 1, relatively high sedimentation rate in the continental rise results in overpressured pore fluids in the uppermost unconsolidated sediments, (b) with a possible contribution of seismic loading, a debris flow occurs at the seafloor, (c) due to the continuous sediment loading, an overpressured zone develops again while the previously formed debris flow becomes buried, and (d) another debris flow takes place at the seafloor. Not to scale. See text for details.

stage, a new debris flow occurs on the seafloor, again with a possible triggering of the local or regional seismic activity (Figure 10d). The process of overpressure zone formation and occurrence of the debris flows continue in this way to form the stacked debrites in the area. The time span between the debrites depends on the formation of the overpressure zone (and hence on the sediment accumulation rate) and the period of seismic loading.

Laboratory experiments proposed by De Blasio et al. (2004) explain the large run-out distances of the debris flows. They showed the subaquous debris flows are of higher velocities and longer run-out distances than subaerial debris flows. This is due to the hydroplaning effect, in which the dynamic pressure at the frontal zone becomes a function of the weight of the sediment involved in the flow (Ilstad et al., 2004; De Blasio et al., 2004). We also conclude that formation of a lubricating water layer beneath the frontal zone due to the hydroplaning reduces the friction along the base of the flow, which contributes to large run-out distances in the study area.

A similar mechanism for the large buried debris lobes offshore Amasra was also proposed by Dondurur et al. (2013) along with a contribution of submarine fluid flow. We do not know the exact timing and sediment composition of the debrites in the area, which needs further investigation with ground-truthing data and C14 dating analysis. As suggested by Dondurur et al. (2013), we conclude that buried debris flows are gravity flows of unconsolidated sediments located in the areas of low slope gradient along the continental rise. In contrast to the debrites offshore Amasra, the flows we observe are in stacked form, which indicates that overpressure conditions in our study area change periodically over the time.

We also propose that the seismicity caused by NAF has a significant effect on the triggering of the debris flows. However, it is not possible to correlate the major events along the NAF with the debris flows in the area. This is because the southernmost edge of the shallowest (and hence, the youngest) debris flow (DB1) is located 20 m depth below the seafloor (assuming a 1600 m/s sediment

velocity), which corresponds to approx. 66,000 years assuming a sedimentation rate of 30 cm/ka. On the other hand, paleoseismological studies on the western part of the NAF are typically concentrated for the time period of the last 2000 years (e.g., Rockwell et al., 2009; Özalp et al., 2013; Drab et al., 2015; Dikbaş et al., 2018). Therefore, it is not possible to correlate the timing of the debris flows with the activity of NAF in the area since there is no information on the seismic activity of NAF at such large time span along the onshore of the study area.

6. Conclusion

High resolution multichannel seismic data show the presence of 14 buried debris lobes in stacked form along the continental rise area between 1400 and 1950 m water depths generally lying in S–to–N direction with run-out distances changing from 3.8 to 24.4 km. The largest debris flow affects a total area of ca. 225 km^2 transporting 15.13 km^3 of sediment. They show the general characteristics of buried debris lobes on the seismic data, such as erosional upper and lower surfaces, lens-shaped form and transparent to chaotic internal structure.

We conclude that the debris flows are gravity flows of unconsolidated sediments located in the areas of low gradient slope along the continental rise. We also suggest that the relatively high sedimentation rate in the area results in excess pore pressures within the underconsolidated subsurface sediments, which is the primary triggering factor along with the seismicity caused by NAF and/or local faulting. That the debrites are in stacked form indicates that the overpressure conditions change periodically over the time. Due to the lack of ground-truthing data, we do not know the exact timing of the debrites. However, relatively small sediment thickness between the stacked debris flows ranging from 8 to 150 m indicates that the time period between the flows may be between 26 and 500 ka considering an average sedimentation rate of 30 cm/ka. The time span between the debrites depends on the formation of the overpressure zone and the period of seismic loading.

Submarine sediment failures are considered as serious geohazards for the settlements of offshore geoengineering structures. Therefore, potentially unstable areas in the region, such as our study area, should be carefully investigated before drilling operations conducted along the margin since the western Black Sea has become a potential region for deep water petroleum exploration in recent years.

Acknowledgments

We would like to thank the captain and the crew of the R/V K. Piri Reis research vessel for their valuable efforts and assistance during the data acquisition. Multichannel seismic data was processed using SeisSpace Promax software of Landmark Graphics and analyzed and interpreted using IHS Kingdom Suite software. We also thank five reviewers for their constructive comments to improve the paper. This work was financially supported by a grant from the Scientific and Technological Research Council of Turkey (TÜBİTAK, project code 108Y110). This study is a part of PhD thesis of Aslıhan Nasıf.

References

Akyüz T, Akyüz S, Bassari A (2001). Radioisotope excited EDXRF analysis of sediment core samples from the southern part of the Black Sea. Journal of Radioanalytical and Nuclear Chemistry 250: 129-137.

Algan O, Gökaşan E, Gazioğlu C, Yücel ZY, Alpar B et al. (2002). A high–resolution seismic study in Sakarya Delta and submarine canyon, southern black sea shelf. Continental Shelf Research 22: 1511-1527.

Alptekin Ö, Nabelek JL, Toksöz MN (1986). Source mechanism of the Bartın Earthquake of September 3, 1968 in northwestern Turkey: evidence for active thrust faulting at the southern Black Sea margin. Tectonophysics 122: 73-88.

Antobreh AA, Krastel S (2007). Mauritania slide complex: morphology, seismic characterisation and processes of formation. International Journal Earth Science 96: 451-472.

Atgın O, Çifci G, Dondurur D, Bialas J, Klaucke I et al. (2014). Investigation of multiple BSR area around offshore of Danube River Channel. In: Gordon Research Conference; Vermont, USA.

Baraza J, Ercilla G, Nelson CH (1999). Potential geologic hazards on the Eastern Gulf of Cadiz Slope (SW Spain). Marine Geology 155: 191-215.

Bilgin T (1984). Adapazarı Ovası ve Sapanca Oluğu'nun Alüvyal Morfolojisi ve Kuvaternerdeki Jeomorfolojik Tekamülü. İstanbul Üniversitesi Yayınları, No. 2572. İstanbul, Turkey: İstanbul Üniversitesi Yayınları, p. 199 (in Turkish).

Bøe R, Hovland M, Instanes A, Rise L, Vasshus S (2000). Submarine slide scars and mass movements in Karmsundet and Skudenesfjorden, Southwestern Norway: morphology and evolution. Marine Geology 167: 147-165.

Casas D, Ercilla G, Baraza J, Alonso B, Maldonado A (2003). Recent mass–movement processes on the Ebro continental slope (NW Mediterranean). Marine and Petroleum Geology 20: 445-457.

Cauchon–Voyer G, Local J, St–Onge G (2008). Late–Quaternary morpho–sedimentology and submarine mass movement of the Betsiamites Area, Lower St. Lawrance Estuary, Quebec, Canada. Marine Geology 251: 233-252.

Çağatay MN (1999). Geochemistry of the Late Pleistocene–Holocene sediments of the Black Sea: an overview. In: Beşiktepe ST, Ünlüata Ü, Bologa AS (editors). Environmental Degradation of the Black Sea: Challenges and Remedies, NATO Science Series, 56. Brussels, Belgium: NATO, pp. 9-22.

Çukur D, Kim S, Kong G, Bahk J, Horozal Ş et al. (2016). Geophysical evidence and inferred triggering factors of submarine landslides on the western continental margin of the Ulleung Basin, East Sea. Geo–Marine Letters 36: 425-444.

De Blasio FV, Engvik L, Harbitz CB, Elverhøi A (2004). Hydroplaning and submarine debris flows. Journal of Geophysical Research 109: 1-15.

Dikbaş A, Akyüz HS, Meghraoui M, Ferry M, Altunel E et al. (2018). Paleoseismic history and slip rate along the Sapanca-Akyazı segment of the 1999 İzmit earthquake rupture (Mw=7.4) of the North Anatolian Fault (Turkey). Tectonophysics 738-739: 92-111.

Diviacco P, Rebesco M, Camerlenghi A (2006). Late Pliocene mega debris flow deposit and related fluid escapes identified on the Antarctic Peninsula continental margin by seismic reflection data analysis. Marine Geophysical Researches 27: 109-128.

Domzig A, Gaullier V, Giresse P, Pauc H, Deverchere J et al. (2009). Deposition processes from echo–character mapping along the western Algerian margin (Oran–Tenes), Western Mediterranean. Marine and Petroleum Geology 26: 673-694.

Dondurur D, Çifçi G (2007). Acoustic structure and recent sediment transport processes on the continental slope of Yeşilırmak River Fan, Eastern Black Sea. Marine Geology 237: 37-53.

Dondurur D, Küçük HM, Çifçi G (2013). Quaternary mass wasting on the Western Black Sea Margin, offshore of Amasra. Global and Planetary Change 103: 248-260.

Drab L, Hubert-Ferrari A, Schmidt S, Martinez P, Carlut J et al. (2015). Submarine Earthquake History of the Çınarcık Segment of the North Anatolian Fault in the Marmara Sea, Turkey. Bulletin of the Seismological Society of America 105 (2A): 622-645.

Drago M (2002). Coupled debris flow–turbidity current model. Ocean Engineering 29: 1769-1780.

Ducassou E, Migeon S, Capotondi L, Mascle J (2013). Run–out distance and erosion of debris–flows in the Nile deep–sea fan system: evidence from lithofacies and micropalaeontological analyses. Marine and Petroleum Geology 39: 102-123.

Dugan B (2012). Petrophysical and consolidation behavior of mass–transport deposits from the northern Gulf of Mexico, IODP Expedition. Marine Geology 315-318: 98-107.

Duman M (1994). Late Quaternary chronology of the Southern Black Sea Basin. Geo–Marine Letters 14: 272-278.

Evans D, King EL, Kenyon NH, Brett C, Wallis D (1996). Evidence for long–term instability in the Storegga slide region off Western Norway. Marine Geology 130: 281-292.

Finetti I, Bricchi G, Del Ben A, Pipan M, Xuan Z (1988). Geophysical study of the Black Sea. Bolletino di Geofisica:Teorica ed Applicata 30: 197-324.

Genov I (2009). Model of palaeoenvironmental evolution of the Black Sea region during the last glacial maximum–Holocene. Oceanology 49: 540-557.

Grozic JLH (2010). Interplay between gas hydrates and submarine slope failure. In: Mosher DC, Shipp RC, Moscardelli L, Chaytor JD, Baxter CDP et al. (editors). Submarine Mass Movements and Their Consequences. Advances in Natural and Technological Hazards Research 28: 11-30.

Hampton MA, Lee HJ, Locat J (1996). Submarine landslides. Reviews in Geophysics 34: 33-59.

Hernández–Molina FJ, Llave E, Ercilla G, Maestro A, Medialdea T et al. (2008). Recent sedimentary processes in the Prestige site area (Galicia Bank, NW Iberian Margin) evidenced by high–resolution marine geophysical methods. Marine Geology 249: 21-45.

Hillman JIT, Klaucke I, Bialas J, Feldman H, Drexler et al. (2018). Gas migration pathways and slope failures in the Danube Fan, Black Sea. Marine and Petroleum Geology 92: 1069-1084.

Hornbach MJ, Manga M, Genecov M, Valdez R, Miller P (2015). Permeability and pressure measurements in Lesser Antilles submarine slides: evidence for pressure–driven slow–slip failure. Journal of Geophysical Research: Solid Earth 120: 7986-8011.

Ilstad T, Elverhøi A, Issler D, Marr JG (2004). Subaqueous debris flow behaviour and its dependence on the sand/clay ratio: a laboratory study using particle tracking. Marine Geology 213: 415-438.

Kenning JJ, Mann P (2020). Control of structural style by large, Paleogene, mass transport deposits in the Mexican Ridges fold–belt and Salina del Bravo, western Gulf of Mexico. Marine and Petroleum Geology 115: 1-18.

Krastel S, Wynn RB, Hanebuth TJJ, Henrich R, Holz C (2006). Mapping of seabed morphology and shallow sediment structure of the Mauritania continental margin, Northwest Africa: some implications for geohazard potential. Norwegian Journal of Geology 86: 163-176.

Kremer CH, McHargue T, Scheucher L, Graham SA (2018). Transversely–sourced mass–transport deposits and stratigraphic evolution of a foreland submarine channel system: Deep–water tertiary strata of the Austrian Molasse Basin. Marine and Petroleum Geology 92: 1-19.

Kret K, Tsuji T, Chhun C, Takano O (2020). Distributions of gas hydrate and free gas accumulations associated with upward fluid flow in the Sanriku–Oki forearc basin, northeast Japan. Marine and Petroleum Geology 116: 104305.

Lee H, Baraza J (1999). Geotechnical characteristics and slope stability in the Gulf of Cadiz. Marine Geology 155: 173-190.

Loncke L, Droz L, Gaullier V, Basile C, Patriat M (2009). Slope instabilities from echo–character mapping along the French Guiana transform margin and Demerara abyssal plain. Marine and Petroleum Geology 26: 711-723.

Menlikli C, Demirer A, Sipahioğlu O, Korpe L, Aydemir V (2009). Exploration plays in the Turkish Black Sea. The Leading Edge 28: 1066-1075.

Middleton GV, Hampton MA (1973). Sediment gravity flows: mechanics of flow and deposition. In: Middleton GV, Bouma AH (editors). Turbidites and Deep Water Sedimentation. Pacific Section SEPM (Society of Economic Paleontologists and Mineralogists), Short Course : 1-38.

Moscardelli L, Wood L (2008). New classification system for mass–transport complexes in offshore Trinidad. Basin Research 20: 73-98.

Mouchot N, Loncke L, Mahieux G, Bourget J, Lallemant S (2010). Recent sedimentary processes along the Makran trench (Makran active margin, off Pakistan). Marine Geology 271: 17-31.

Mulder T, Gonthier E, Lecroart P, Hanquiez V, Marches E (2009). Sediment failures and flows in the Gulf of Cadiz (Eastern Atlantic). Marine and Petroleum Geology 26: 660-672.

Nasıf A, Dondurur D (2017). The morpho–acoustic structure of Sakarya Canyon, southwestern Black Sea. In: 19th European Geosciences Union (EDU) General Assembly; Vienna, Austria. p. 12079.

Nasıf A, Özel FE, Dondurur D (2019). Morphology and recent sediment distribution along the Sakarya Canyon: preliminary results from seismic data. In: 72. Turkish Geological Congress; Ankara, Turkey.

Nasıf A, Özel FE, Dondurur D (2020). Seismic identification of gas hydrates: a case study from Sakarya Canyon, Western Black Sea. Turkish Journal of Earth Sciences, 29: 434-454.

Nikishin AM, Okay A, Tüysüz O, Demirer A, Wannier M (2015). The Black Sea basins structure and history: New model based on new deep penetration regional seismic data. Part 2: Tectonic history and paleogeography. Marine and Petroleum Geology 59: 656-670.

Okay AI, Şengör AMC, Görür N (1994). Kinematic history of the opening of the Black Sea and its effect on the surrounding regions. Geology 22: 267-270.

Özalp S, Emre Ö, Doğan A (2013).The segment structure of southern branch of the North Anatolian Fault and paleoseismological behaviour of the Gemlik fault, NW Anatolia. Bulletin of the Mineral Research and Exploration 147: 1-17.

Reece JS, Flemings PB, Dugan B, Long H, Germaine JT (2012). Permeability–porosity relationships of shallow mudstones in the Ursa Basin, northern deepwater Gulf of Mexico. Journal of Geophysical Research 117: B12102.

Robinson AG, Rudat JH, Banks CJ, Wiles RLF (1996). Petroleum geology of the Black Sea. Marine and Petroleum Geology 13: 195-223.

Rockwell T, Ragona D, Seitz G, Langridge R, Aksoy ME et al. (2009). Palaeoseismology of the North Anatolian Fault near the Marmara Sea: implications for fault segmentation and seismic hazard. In: Reicherter K, Michetti AM, Silva PG (editors). Palaeoseismology: Historical and Prehistorical Records of Earthquake Ground Effects for Seismic Hazard Assessment. The Geological Society, London, Special Publications 316: 31-54.

Ross DA (1977). The Black Sea and the Sea of Azov. In:Nairn AEM, Kanes WH, Stehli FG (editors). The Ocean Basins and Margins. New York, NY, USA: Plenum Publications, pp. 445-481.

Rovere M, Gamberi F, Mercorella A, Leidi E (2014). Geomorphometry of a submarine mass–transport complex and relationships with active faults in a rapidly uplifting margin (Gioia Basin, NE Sicily margin). Marine Geology 356: 31-43.

Savini A, Corselli C (2010). High–resolution bathymetry and acoustic geophysical data from Santa Maria di Leucacold water coral province (Northern Ionian Sea–Apulian continental slope). Deep–Sea Research–II 57: 326-344.

Shanmugam G (1996). High–density turbidity currents; are they sandy debris flows? Journal of Sedimentological Research 66: 2-10.

Shanmugam G (2000). 50 years of the turbidite paradigm (1950s–1990s): deep–water processes and facies models–critical perspective. Marine and Petroleum Geology 17: 285-342.

Shanmugam G (2016). Submarine fans: a critical retrospective (1950–2015). Journal of Palaeogeography 5: 110-184.

Sipahioğlu NÖ, Batı Z (2017). Messinian canyons in the Turkish western Black Sea. In: Simmons MD, Tarı GC, Okay AI (editors). Petroleum Geology of the Black Sea. Geological Society, London, Special Publications: 464.

Sultan N, Cochonat P, Canals M, Cattaneo A, Dennielou B et al. (2004). Triggering mechanisms of slope instability processes and sediment failures on continental margins: a geotechnical approach. Marine Geology 213: 291-321.

Sun Q, Leslie S (2020). Tsunamigenic potential of an incipient submarine slope failure in the northern South China Sea. Marine and Petroleum Geology 112: 104-111.

Sun Q, Alves T (2020). Petrophysics of fine–grained mass–transport deposits: A critical review. Journal of Asian Earth Sciences 192: 104291.

Sun Q, Alves TM, Lu XY, Chen CX, Xie XN (2018). True volumes of slope failure estimated from a Quaternary mass–transport deposit in the northern South China Sea. Geophysical Research Letters 45: 2642-2651.

Talling PJ, Masson DG, Sumner EJ, Malgesini G (2012). Subaqueous sediment density flows: depositional processes and deposit types. Sedimentology 59: 1937-2003.

Tarı E, Şahin M, Barka A, Reilinger R, King RW et al. (2000). Active tectonics of the Black Sea with GPS. Earth Planets Space 52: 747-751.

Tarı G, Fallah M, Kosi W, Floodpage J, Baur J et al. (2015). Is the impact of the Messinian Salinity Crisis in the Black Sea comparable to that of the Mediterranean?Marine and Petroleum Geology 66: 135-148.

Von Huene R, Ranero CR, Watts P (2004). Tsunamigenic slope failure along the Middle America Trench in two tectonic settings. Marine Geology 203: 303-317.

Wilken M, Mienert J (2006). Submarine glacigenic debris flows, deep–sea channels and past ice–stream behaviour of the East Greenland continental margin. Quaternary Science Reviews 25: 784-810.

Winguth C, Wong HK, Panin N, Dinu C, Georescu P et al. (2000). Upper Quaternary water level history and sedimentation in the northwestern Black Sea. Marine Geology 167: 127-146.

Yang T, Cao Y, Liu K, Wang Y, Zavala C et al. (2019). Genesis and depositional model of subaqueous sediment gravity–flow deposits in a lacustrine rift basin as exemplified by the Eocene Shahejie Formation in the Jiyang Depression, Eastern China. Marine and Petroleum Geology 102: 231-257.

Yiğitbaş E, Elmas A, Sefunç A, Özer N (2004). Major neotectonicfeatures of eastern Marmara region, Turkey: development of the Adapazarı–Karasu corridor and its tectonic significance. Geological Journal 39: 179-198.

Zonenshain LP, Le Pichon X (1986). Deep basins of the Black Sea and Caspian Sea as remnants of Mesozoic back–arc basins. Tectonophysics 123: 181-211.